

Inclusive Photoproduction of η Mesons on Nuclei and the in-medium properties of the S_{11} Resonance *

M. Hedayati-Poor^{a,b} and H.S. Sherif^a

(a)Department of Physics, University of Alberta
Edmonton, Alberta, Canada T6G 2J1

(b)Department of Physics, University of Arak, Iran

November 13, 2018

Abstract

A relativistic non-local model for the inclusive photoproduction of η mesons from complex nuclei is introduced. The model is based on the dominance of the $S_{11}(1535)$ resonance. We compare the results of our calculations with the available data on inclusive cross sections for the nuclei C, Al and Cu. Assuming the resonance propagates freely in the nuclear medium, we find that the calculated angular distribution and energy dependence of the cross sections reproduce the data in a reasonable fashion. The present non-local model allows the inclusion of density dependent mass and width in the calculations. Including these in the calculations reveals that the presently available data do not show clear preference for the inclusion of such modifications of the properties of the $S_{11}(1535)$ in the nuclear medium.

PACS number(s) 25.20.Lj, 24.10.Jv, 14.20.Gk, 13.60.Le

*Work supported in part by the Natural Sciences and Engineering Research Council of Canada

1 Introduction

The question of possible modifications of hadron properties in the nuclear medium has attracted considerable interest in recent years. This interest stems from the hope that studies of these effects can clarify the interplay of the competing degrees of freedom in the nucleus. In particular it may be possible to learn about explicit quark degrees of freedom in the nucleus through such studies.

There have been several theoretical as well as experimental investigations of these effects, and evidence is gathering that indeed such modifications do take place. Several studies have been carried out for the modifications of meson properties in heavy ion and other collisions [1, 2, 3, 4, 5]. Photonuclear reactions also lend themselves to investigations of this type [6, 3, 7]. In particular, a promising area of investigation is the photoproduction of η mesons on nuclei in the energy range corresponding to the second resonance region of the nucleon. The fact that one resonance, the $S_{11}(1535)$, dominates the production process at these energies, makes it attractive to look at these reactions for clues on changes in its properties in the nuclear medium.

Three pioneering and complementary measurements of the inclusive eta photoproduction on nuclei have been reported in recent years. The earlier measurements of Robig-Landau *et al* [8] at MAMI included cross sections on a number of nuclei from threshold up to a photon energy of 800 MeV. These cross sections displayed the expected rise on the low energy side of the resonance. Few years later measurements of the same reaction were performed at KEK [9], extending the energy range to 1GeV. This group reported that a broad resonance due to the excitation and decay of the S_{11} resonance in the nucleus has been observed for the first time. In a recent investigation, Kinoshita *et al* [10] reported on measurements of this reaction on C and Cu targets at LNS, for photon energies up to 1.1 GeV. These authors indicated the importance of the contributions from other nucleon resonances in the second resonance region in addition to the dominant S_{11} , at energies higher than 900 MeV. The authors of references [9, 10] performed calculations for their data using an adaptation of the Quantum Molecular Dynamics model. Lehr *et al* [11] performed calculations based on the semi-classical BUU transport model. Another approach was that of Maruyama and Chiba [12] who carried out relativistic calculations in infinite nuclear matter based on an effective Lagrangian and a scaling factor to account for

the final state interactions of the η mesons.

In the present paper we present an analysis of the data based on a relativistic model for the inclusive photoproduction on finite nuclei. The main ingredients of model are the use of an effective Lagrangian approach (Benmerrouche *et al*[13]) and the relativistic mean field approach to nuclear dynamics [14]. The final state interactions of the outgoing η meson are taken into account. This fully non-local model has been discussed recently for the cases of exclusive and incoherent photoproduction [15, 16]. These non-local calculations, in contrast to earlier local ones [17], allow us to include possible density dependent changes in the mass and width of the resonances in the nuclear medium.

The justification for the claim that the inclusive data from KEK, Mainz and LNS may reveal changes in the properties of the S_{11} resonance requires some discussion. It is known that the S_{11} is the main contributor to the η photoproduction cross section on free nucleons in the 0.6 - 1GeV range. There are contributions from neighboring resonances and from nucleon Born terms as well as meson exchange diagrams; but these are small by comparison. We will show in the course of our discussion that this situation carries over to the inclusive production on nuclei. The contributions are only at the few percent level, a situation which allows us to probe whether the existing data does reveal any information regarding the properties of the S_{11} in the medium. As we shall show there are remaining uncertainties regarding other aspects of the analysis which are more important compared to the small contributions of other diagrams.

The plan of the paper follows a recent discussion of the non-local relativistic model for the exclusive quasifree photoproduction of η mesons. The reaction amplitude is cast in a general form in section 2 where the method of evaluation of the amplitude in its non-local form is outlined. The results of the model and the discussion are given in section 3. Conclusions are given in section 4.

2 Formalism

In the inclusive reaction, a photon is absorbed by the nucleus and as a result an η meson is produced. This meson is the only detected particle and there is no information about the final state of the nuclear system. In the present

work it is assumed that the inclusive reaction is based on the exclusive reaction in which a single nucleon is ejected in the continuum in the course of the production process [18, 19]. The transition amplitude for the exclusive reaction through the S_{11} resonance, in its full non-local form, is given by [15],

$$\begin{aligned}
S_{fi} = & \frac{e}{(2\pi)^{17/2}} \frac{\kappa_R g_{\eta NR}}{M + M_R} \left(\frac{M}{E_N} \frac{1}{2\omega_\eta} \frac{1}{2\omega_\gamma} \right)^{1/2} & (1) \\
& \times \sum_{J_B M_B} (J_f, J_B; M_f, M_B | J_i, M_i) [S_{J_i J_f}(J_B)]^{\frac{1}{2}} \\
& \times \left\{ \int d^4x d^4y d^4p \bar{\psi}_{sf}(y) \phi_\eta^*(y) \frac{e^{-ip(y-x)}}{\not{p} - M_R + i\frac{\Gamma}{2}} \gamma_5 \not{k}_\gamma \not{\epsilon} e^{-ik_\gamma x} \psi_B(x) \right. \\
& \quad \left. + \int d^4x d^4y d^4p \bar{\psi}_{sf}(y) \gamma_5 \not{k}_\gamma \not{\epsilon} e^{-ik_\gamma y} \frac{e^{-ip(y-x)}}{\not{p} - M_R + i\frac{\Gamma}{2}} \phi_\eta^*(x) \psi_B(x) \right\},
\end{aligned}$$

where E_N , ω_η and ω_γ are the energies of the final nucleon, η meson and incident photon, respectively. M is the nucleon mass, M_R and Γ represent the mass and width of resonance. $S_{J_i J_f}(J_B)$ and $(J_f, J_B; M_f, M_B | J_i, M_i)$ are spectroscopic and Clebsh-Gordon coefficients. κ_R and $g_{\eta NR}$ are the anomalous magnetic moment of the resonance and its coupling constant with η and nucleon. $\psi_{sf}(y)$, $\psi_B(y)$ and $\phi_\eta(y)$ are wave functions describing the final nucleon, initial nucleon and η meson, respectively. $\psi_B(y)$ is a solution of the Dirac equation with appropriate mean field potentials and ϕ_η is a solution of the Klein - Gordon equation. As is explained in [19], the wave function of the final nucleon ($\psi_{sf}(y)$) is taken to be a plane wave. Calculations without inclusion of the final state interaction of η meson revealed that the u-channel contribution (second term in (1)) is less by two orders of magnitude than that of s-channel (first term in (1)). As a result the non-locality and possible medium modifications of the former will have a negligible effect on the calculated cross section. We thus ignore this very small change and treat the u-channel locally as in [19]. The dominant s-channel diagram is treated in the non-local approach.

The medium modifications of the properties of the nucleon resonance are often expressed in terms of changes of its mass and width from their free values in a manner dependent on the nuclear density [20, 11]. Our non-local approach can accommodate these density dependent parameters for the resonance. After implementing the density dependent mass and width

for the resonance in the s-channel part of the above amplitude, we calculate the resulting integral following an approach similar to the one used in ref.[21]. We rewrite the integral of the s-channel part in eq(1) as

$$(2\pi)^4 \int d^4y \chi_{sf}^\dagger \left(1 + \frac{\boldsymbol{\sigma} \cdot \mathbf{k}_N}{E_N + M}\right) e^{ik_N y} \phi_\eta^*(y) W(y), \quad (2)$$

where we use a plane wave function (see ref. [19]) for the final state of the struck nucleon; χ_{sf} denotes its spin state. The function $W(y)$ has the following form

$$(2\pi)^4 W(y) = \int d^4x d^4p \frac{e^{-ip(y-x)}}{\not{p} - M_R(\rho) + i\frac{\Gamma(\rho)}{2}} \gamma_5 \not{k}_\gamma \not{p} e^{-ik_\gamma x} \psi_B(x). \quad (3)$$

Acting with the operator $\not{p} - M_R(\rho) + i\frac{\Gamma(\rho)}{2}$ (ρ refers to the density of the nucleus) from the left on (3) and then carrying the integration over momentum, the following Dirac-type linear differential equation is obtained

$$\left(\not{p} - M_R(\rho) + i\frac{\Gamma(\rho)}{2}\right) W(y) = V(y), \quad (4)$$

where the source term is

$$V(y) = \gamma_5 \not{k}_\gamma \not{p} e^{-ik_\gamma y} \psi_B(y). \quad (5)$$

Equation (4) leads to the following second order differential equation for the the upper component of $W(\mathbf{r})$.

$$[\mathbf{p}^2 - \alpha(r)\beta(r)]W_{up}(\mathbf{r}) = \boldsymbol{\sigma} \cdot \mathbf{p}V_d(\mathbf{r}) - \beta(r)V_{up}(\mathbf{r}), \quad (6)$$

where the indices up and d indicate the upper and lower components of the functions $W(\mathbf{r})$ and $V(\mathbf{r})$. Note these functions continue to be spin dependent. The lower component $W_d(\mathbf{r})$ can be obtained from the upper component as,

$$W_d(\mathbf{r}) = \frac{\boldsymbol{\sigma} \cdot \mathbf{p}W_{up}(\mathbf{r}) - V_d(\mathbf{r})}{\beta(r)}. \quad (7)$$

The functions $\alpha(r)$ and $\beta(r)$ are

$$\begin{aligned} \alpha(r) &= E_b + w_\gamma - M_R(\rho) + i\frac{\Gamma(\rho)}{2} \\ \beta(r) &= E_b + w_\gamma + M_R(\rho) - i\frac{\Gamma(\rho)}{2}, \end{aligned} \quad (8)$$

where E_b is the energy of the bound nucleon. $W_{up}(\mathbf{r})$ is obtained by solving eq.(6) following the same approach as in ref.[15].

Substituting the solution of $W_{up}(\mathbf{r})$ into eq.(1) we get,

$$S_{fi} = \frac{e}{\pi} \left(\frac{E_p + M}{E_p \omega_\eta \omega_\gamma} \right)^{1/2} \frac{\kappa_R g_{\eta NR}}{M + M_R} \delta(E_B + \omega_\gamma - E_p - \omega_\eta) \quad (9)$$

$$\times \sum_{J_B M_B} (J_f, J_B; M_f, M_B | J_i, M_i) \left[\mathcal{S}_{J_i J_f}(J_B) \right]^{1/2} (Z_{s_f M_B}^s + Z_{s_f M_B}^u)$$

The transition function for the u-channel $Z_{s_f M_B}^u$ is calculated in the local approximation and is the same as eq.(3) in [19]. The corresponding function for the s-channel is calculated in non-local approach described above and is

$$Z_{s_f M_B}^s = \frac{1}{(4\pi)^{\frac{1}{2}}} \sum_{L J M L_\eta, M_\eta} i^{-(L+L_\eta)} Y_L^{M-s_f}(\hat{\mathbf{k}}_f) \left[Y_{L_\eta}^{M_\eta}(\hat{\mathbf{k}}_\eta) \right]^* \quad (10)$$

$$\times (L, 1/2; M - s_f, s_f | J, M)$$

$$\times \int d^3r \left[\mathcal{Y}_{L,1/2,J}^M(\Omega) \right]^* v_{L_\eta}(r) Y_{L_\eta}^{M_\eta}(\Omega) (W_u(\mathbf{r}) - \frac{\sigma \cdot \mathbf{k}_f}{E_N + M} W_d(\mathbf{r}))$$

where $v_{L_\eta}(r)$ is the radial wave function of the η meson. $\hat{\mathbf{k}}_f$ and $\hat{\mathbf{k}}_\eta$ are unit vectors along the directions of the final nucleon and η meson, respectively. The amplitude (9) is used to calculate the cross section for the exclusive reaction (see eq(5) of ref.[19]) . The inclusive cross section is obtained by numerical integration of the exclusive cross section over the phase space of the final nucleon and summing over all energy levels of the target nucleus.

In the following section we shall explore whether the available data can be used to clarify the issue of possible modifications of the mass and width of the S_{11} resonance. For this purpose we will adopt phenomenological forms of these parameters suggested by earlier works [20, 11]. For mass we use a density dependent form suggested by the quark-meson coupling model for hadrons [20].

$$M(\rho) = M_{\text{free}} \left(1 - b \frac{\rho}{\rho^0} \right) \quad (11)$$

For width we use a density dependent form given in [11] which includes the broadening of the resonance width due to its collisions with hadrons in the medium,

$$\Gamma(\rho) = \Gamma_{\text{free}} + c \frac{\rho}{\rho^0}, \quad (12)$$

3 Results and Discussion

Throughout the calculations presented here we use scalar and vector potentials of Woods Saxon form to generate the bound state Dirac wave functions of the nucleons. The parameters of these potentials for different targets are listed in table 1. The final state interactions of the eta meson are taken into account through the use of the optical potential DW1 from ref.[22]. For the coupling to the proton we use the parameters of set 3 given in table 1 of ref.[23] and in calculating the neutron contributions we use the factor $\frac{2}{3}$ for the ratio of neutron to proton cross sections.

It is well known that the photoproduction process on the nucleon, in the second resonance region, is dominated by the $S_{11}(1535)$ diagram. We begin our discussion by showing that this situation carries over to the inclusive reactions on nuclei. The collective contributions from other diagrams are small by comparison. This is shown in Fig.1. Figure 1(a) shows the angular distribution of the inclusive cross section of the reaction on ^{12}C at a photon incident energy $E_\gamma = 820$ MeV. The solid curve gives the S_{11} contribution while the dashed curve includes the additional contributions due to the D_{13} , the nucleon pole terms and the meson exchange diagrams.

The total inclusive cross section on ^{12}C for photon energies in the range 0.65 - 1.1 GeV is depicted in Fig.1(b). The dominance of the S_{11} contributions is clearly evident from these comparisons. It is worth mentioning here that this rather fortunate circumstance arises not only from the relative smallness of the contributions of the other diagrams, but also from strong cancellations among these contributions.

Fig.2 shows the inclusive angular distributions for C, Al and Cu. For each target nucleus, we show the distributions at two photon energies from among those measured: 740 MeV and 980 MeV. The data are those of KEK [9], LNS [10] and MAINZ (only for ^{12}C at 740 MeV) [8]. The solid curves represent non-local calculations that assume free propagation for the S_{11} resonance. We take the free mass and width of the resonance to be 1535 MeV and 160 MeV, respectively. In these and subsequent figures these curves are labeled 'Free'. General trends in the data are reproduced and the agreement is almost quantitative in some cases. The main exception is the case of Al at 980 MeV. There are some disagreements among the measurements from KEK and LNS in the case of Cu and our theoretical calculations show better agreement with the latter measurements.

The dashed curves in Fig. 2 represent calculations in which, following suggestions of ref.[11], the width of the S_{11} resonance is assumed to undergo density dependent broadening in the medium of the form given in eq(12) with $c = 50$ MeV. We note that the broadening leads to reduction in the cross sections for all three nuclei. It may be argued that the effect leads to a worsening in the accord with the data for C at the lower energy (740 MeV) and by contrast to a slight improvement at 980 MeV. For Al the quality of agreement with the data remains about the same, whereas for Cu, the disagreement between measurements makes it difficult to judge the outcome.

We now consider the effect of a reduction of mass on the angular distributions. In the discussion of ref.[20], the authors suggested that the nucleon mass in the medium is reduced according to eq.(11) with a value of the reduction parameter $b = 0.14$. Fig.3 shows the results of the angular distribution for the same targets and photon energies as in Fig.2. The dash-dotted curves are obtained when the above value is used for the reduction of the mass of the S_{11} . Compared to calculations with no medium effects (solid curves), we note a large decrease in the cross section. This also brings the calculated cross section much below the data. This clearly indicates that if the mass of the S_{11} were reduced in the medium, the scale of reduction would be much smaller than is indicated by the value of b given above. If the reduction in mass is made weaker the effect becomes smaller. For example the dashed curves show the calculations for a much smaller value of b ($b = 0.014$). Here the effect on the cross section is relatively small. We note that at the lower energy the effect leads to a slight increase in the magnitude of the cross section while the effect at the higher energy is a slight decrease.

The data for the total inclusive cross section (obtained by integrating the angular distributions discussed above) are shown in Figs.4-6. These include the data for the three nuclei C, Al and Cu from KEK, Mainz and LNS. Fig.4 displays the inclusive data for C. In Fig.4(a) we show the effects of changes in the mass of the S_{11} on the behavior of the total inclusive cross section in the energy range from near threshold to 1.1 GeV. The solid curve represents the case of no medium modification of the mass. We note that these calculations provide reasonable agreement with the data particularly over and beyond the peak, but are slightly lower at the lower energies. The dashed and dash-dotted curves represent the two cases where the mass modification parameter b of eq.(11) has the values 0.014 and 0.035, respectively. The latter value, though it improves the accord with the data on the lower energy side of the

peak somewhat, still gives a strong suppression on the higher energy side. Calculations with the smaller value of b lie below the data at energies above 900 MeV.

In Fig.4(b) we present similar comparisons involving changes to the width of the resonance. We show two cases for density dependent changes in the width of the form given in eq.(12). The dash-dotted curve is for a value of $c = 25$ MeV and the dashed curve is for $c = 50$ MeV. Both these calculations lead to a lowering of the cross section away from the data.

Figs.5 shows similar comparisons for the KEK inclusive cross section on Al and Fig.6 compares the calculations with the KEK and LNS data for Cu. The qualitative features of the results are similar. Again the data rule out any strong reduction (associated with $b = 0.14$) in the mass of the resonance. A reduction in the mass of S_{11} corresponding to a value of $b = 0.014$ brings the calculations somewhat closer to the data for Al, but leads to a reduced cross section at higher energies for Cu. In the case of the modification of width we note that the density dependent width of eq.(12), with $c = 50$ MeV, leads to a suppression of the cross section away from the data.

We have argued earlier that the dominance of the S_{11} contributions is used to limit the forgoing comparisons and discussions to this contribution. In fig 7 we revisit this question. In part (a) we show the results for the case of production on C for the S_{11} . We compare this with the results in the lower panel (b) based on calculations in which the small contributions from the D_{13} , the nucleon pole and the t-channel vector meson diagrams are included. These contributions, being small, are calculated using the local approximation (the non-local corrections in this case are expected to be negligible). Each of the curves in panel (a) has a counterpart in panel (b): The solid curves represent the free calculations, the dashed curves represent calculations in which the mass reduction is affected by a value $b = 0.014$. The dash-dotted curves represent calculations in which we make changes in both mass and width of the resonance. We assumed the width is reduced to 150 MeV (from 160 MeV) and in the meantime the mass is reduced as above. It is seen from the figures that the inclusion of the additional contributions, though it modifies the cross section slightly, does not alter the character of the comparison with the data, from those involving only the S_{11} contributions.

The preceding comparisons were based on calculations using the optical potential DW1 to describe the final state interaction of the η meson. The calculations of the cross sections are sensitive to the optical potential used.

For example we show in Fig.8 a comparison of the cross sections calculated using one of the optical potentials derived by Oset *et al.*[24]. These calculations of the eta optical potential depend on the magnitude of the real part of S_{11} self energy in the medium, and we have used the case for which the real part of the S_{11} self-energy is -50 MeV. The cross sections are seen to lie below those calculated using the DW1 potential. It is clear that this type of uncertainty should be kept in mind before a final verdict is gleaned from the data as to the extent of any medium modifications of the properties of the resonance.

4 conclusion

A relativistic non-local model for the inclusive photoproduction of η mesons from complex nuclei is introduced. This model is based on the dominance of the contributions due to the formation of the S_{11} resonance. The inclusion of non-local effects is the main improvement over our earlier work which was applied to the limited data available at the time. Moreover, the non-local approach makes it possible to include mass and width parameters of the resonance that may depend on the nuclear density.

Calculations were first carried out using the free mass and width for the resonance (i.e. no medium effect). Comparison of the results of these calculations with the data available for C, Al and Cu, reproduce the overall shape of the angular distributions as well as the total cross section data up to 1.0 GeV. It is worth noting that our results are in somewhat better agreement with the recent data of LNS than with the older data.

The influence of possible medium modifications of the properties of the resonance was also studied. Simple density dependent forms for the mass and width of the resonance were used to test the effect these have on the calculated cross sections and their accord with the data. Comparison with the data showed that reductions in the mass of S_{11} on a scale similar to that suggested for the nucleon leads to cross sections that disagree strongly with the data. The data can accommodate much weaker changes in the mass and some broadening of the width. Although one can claim some scattered instances of improvement with these changes, it is not possible to claim that the data show clear evidence of medium modifications of resonance parameters. The lack of this evidence is due in part to the occasional disagreement between different

measurements. There is also the inherent weakness in our present knowledge of the final state interaction of the eta meson with nuclei (represented here by the optical potential), which adds to the uncertainty. In conclusion we would estimate that if any medium modifications of the properties of the S_{11} resonance existed, they would likely be rather small. This is in agreement with the general conclusions reached by the authors of refs.[7, 10, 11, 12].

Acknowledgments

We Would like to thank T. Yorita and T. Kinoshita for their helpful communications regarding their data. We also are grateful to E. Sumber, from Computing and Network Services at University of Alberta for parallelizing our computer code and to West Grid for allowing us to use their facilities to perform our computations. This work was supported in part by the Natural Sciences and Engineering Research Council of Canada.

References

- [1] G.E. Brown and M. Rho, Phys. Rev. Lett **66**(1991)2720; Phys. Rep. 398 (2004)301.
- [2] Bi Pin-zhen and J Rafelski, nucl-th/0507037
- [3] U. Mosel, nucl-th/0507050
- [4] K. Saito, K. Tsushima and A.W. Thomas hep-ph/0506314
- [5] D. Adamvoá *et al.*, Phys. Rev. Lett **91**(2003) 042301.
- [6] CBELSA/TAPS Collaboration, Phys. Rev. Lett **94**(2005)192303.
- [7] B. Krusche, Acta Phys. Hung. **A 19**(2004)000-000.
- [8] M. Roebig-Landau *et al.*, Phys. Lett. **B373** (1996) 45.
- [9] T. Yorita *et al.*, Phys. Lett. **476** (2000) 226; H. Yamazaki *et al.*, Nucl. Phys. **A670**, (2000)202.
- [10] T. Kinoshita *et al.*,nucl-ex/0509022.

- [11] J. Lehr, M. Post and U. Mosel, Phys. Rev. **C68** (2003) 044601: J. Lehr and U. Mosel, Phys. Rev. **C68** (2003)044603:
- [12] T. Maruyama and S. Chiba, Prog. Theo. Phys. **111**(2004)229.
- [13] M. Benmerrouche, Nimai C. Mukhopadhyay, and J.F. Zhang, Phys. Rev. **D51**, (1995) 3237
- [14] B.D. Serot and J.D. Walecka, *Advances in Nuclear Physics*, edited by J.W. Negele and E. Vogt, **16**(1986)1.
- [15] M. Hedayati-Poor, S. Bayegan and H.S. Sherif, Phys. Rev. **C68**, (2003) 045205.
- [16] M. Hedayati-Poor and H.S. Sherif, Nucl. Phys. **A740**, (2004) 309.
- [17] M. Hedayati-Poor and H.S. Sherif, Phys. Rev. **C56**, (1997) 1557.
- [18] C. Bennhold, H. Tanabe, Nucl. Phys. **A530**(1991)625.
- [19] M. Hedayati-Poor and H.S. Sherif, Phys. Rev. C **58** (1998) 326.
- [20] K. Saito and A. W. Thomas, Phys. Rev. **C51** (1995)2757.
- [21] E.D. Cooper and O.V. Maxwell , Nucl. Phys. **A493**, (1989) 486.
- [22] F.X. Lee, L.E. Wright, C. Bennhold and L. Tiator, Nucl. Phys. **A603** (1996) 345.
- [23] I.R. Blokland and H.S. Sherif, Nucl. Phys. **A694** (2001) 337.
- [24] H.C. Chiang, E. Oset and L.C. Liu, Phys. Rev. **C44** (1991)738.

Table Caption

TABLE 1. Strengths, reduced radii and diffuseness for the relativistic scalar and vector mean-field potentials, respectively.

Figure Captions

FIG. 1. Differential (a) and total (b) inclusive cross section for $^{12}\text{C}(\gamma, \eta)$ reaction. Solid curves: S_{11} resonance contribution, dashed curves: Sum of contributions from S_{11} resonance, D_{13} resonance, nucleon pole and vector meson.

FIG. 2. Differential inclusive cross section for (γ, η) reaction on C, Al and Cu nuclei. The graphs in the left and right panels represent the results for incident photon energies of $E_\gamma = 740$ MeV and $E_\gamma = 980$ MeV, respectively. Solid curves: calculations using the values 1535 MeV and 160 MeV for the mass and width of S_{11} resonance, respectively (labeled Free in this and subsequent figures), dashed curves: density dependent width of eq(12) with $c = 50$ MeV (labeled $\Gamma(\rho)$). Optical potential DW1 of ref.[22] is used. Data are (KEK) from [9], (LNS) from [10] and (MAINZ) from [8].

FIG. 3. Same as Fig.2, but for the effect of mass modifications. Solid curves: free calculations, dashed curves: density dependent mass of eq(11) with $b = 0.014$, dash-dotted curves: density dependent mass of eq(11) with $b = 0.14$.

FIG. 4. Total inclusive cross section for the $^{12}\text{C}(\gamma, \eta)$ reaction. Data and potentials are from the same references as in Fig.2. Fig.4(a); solid curve: free calculations, dashed curve: density dependent mass of eq(11) with $b=0.014$, dash-dotted curve: density dependent mass of eq(11) with $b=0.035$. Fig.4(b); solid curve: free calculation, dashed curve: density dependent width of eq(12) with $c = 50$ MeV, dash-dotted curve: density dependent width of eq(12) with $c = 25$ MeV.

FIG. 5. Same as Fig.4 but for Al. In Fig.5(a): solid curve: free calculations, dashed curve: density dependent mass of eq(11) with $b=0.014$, dash-dotted curve: density dependent mass of eq(11) with $b=0.14$. In Fig.5(b): solid curve: free calculations, dashed curve: density dependent width of eq(12) with $c = 50$ MeV, data are those of ref.[9].

FIG. 6. Same as Fig.5 but for Cu. Curves are labeled same as Fig.5. Data are: (KEK) and (LNS) from refs. [9] and [10], respectively.

FIG. 7. Same as Fig.4. Curves in panel (a) are contributions from S_{11} resonance, solid curve: free calculations, dashed curve: free width of 160 MeV and density dependent mass of eq(11) with $b=0.014$, dash-dotted curve: free width of 150 MeV and density dependent mass of eq(11) with $b=0.014$. The contributions of nucleon poles, D_{13} resonance and vector meson diagrams are added to the ones for S_{11} in the calculations presented in panel(b). Curves are labeled as in panel(a).

FIG. 8. Same as the free calculations in Fig.4 (S_{11} resonance contributions only). Solid curve: using optical potential DW1 of ref.[22], dashed curve: using optical potential of ref.[24] with the real part of the S_{11} self-energy set to -50 MeV.

Nucleus	V_v MeV	r_v (fm)	a_v (fm)	V_s (MeV)	r_s (fm)	a_s (fm)
^{12}C	385.7	1.056	0.427	-470.4	1.056	0.447
^{27}Al	354.1	1.09	0.450	-444.5	1.09	0.500
^{63}Cu	348.1	1.149	0.476	-424.5	1.149	0.506

Table 1:

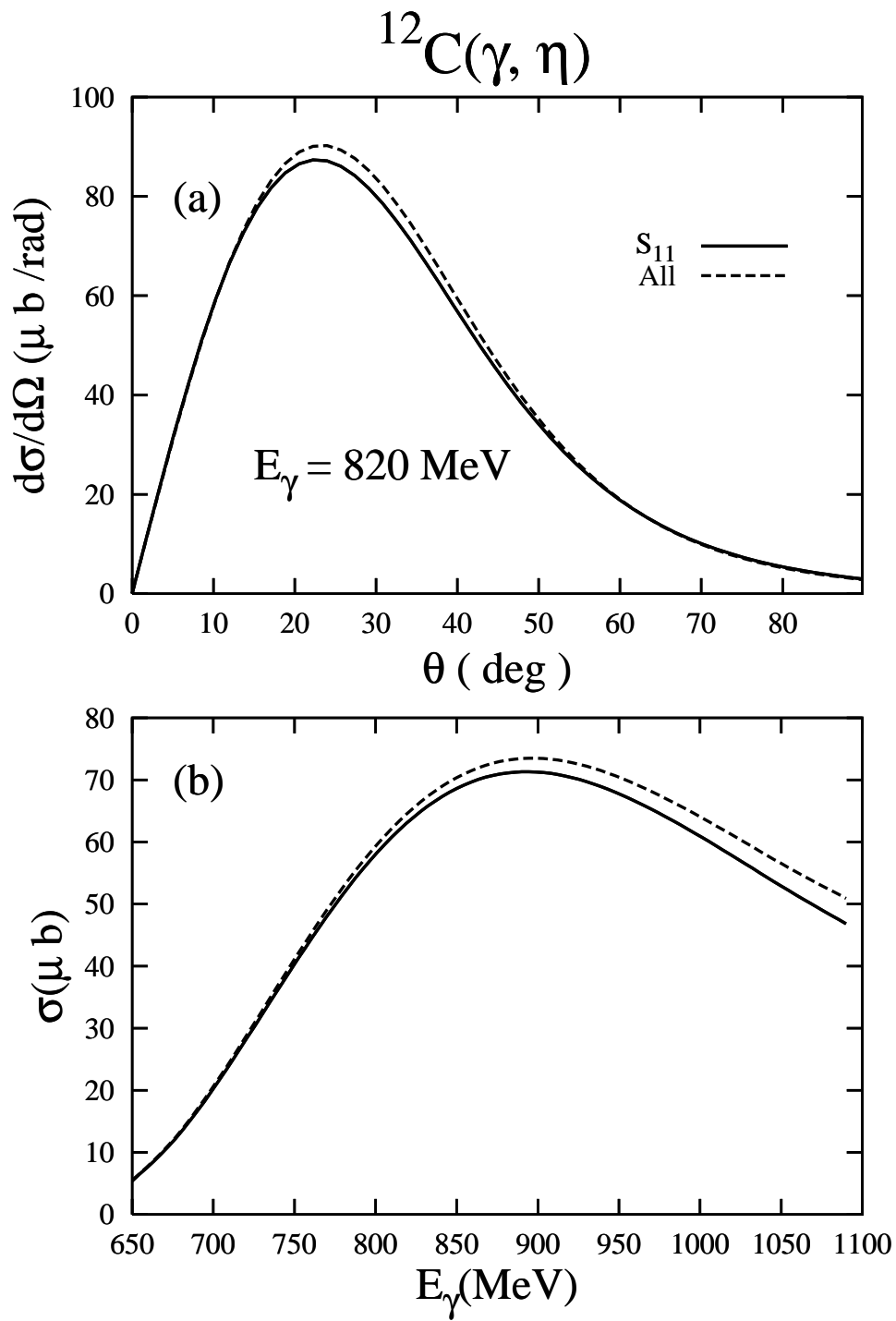


Fig.1

(γ, η)

$E_\gamma = 740 \text{ MeV}$

$E_\gamma = 980 \text{ MeV}$

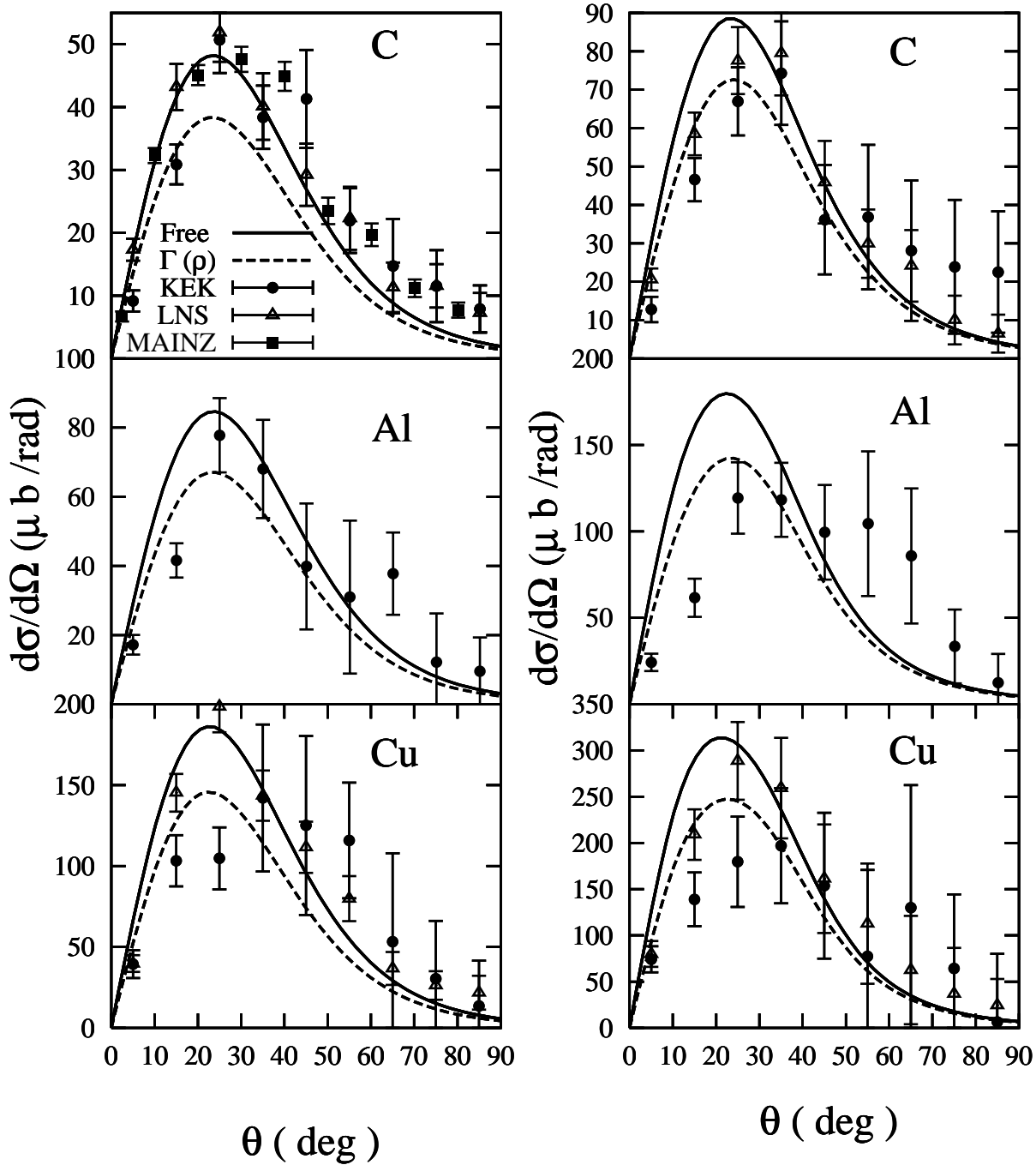


Fig.2

(γ, η)

$E_\gamma = 740 \text{ MeV}$

$E_\gamma = 980 \text{ MeV}$

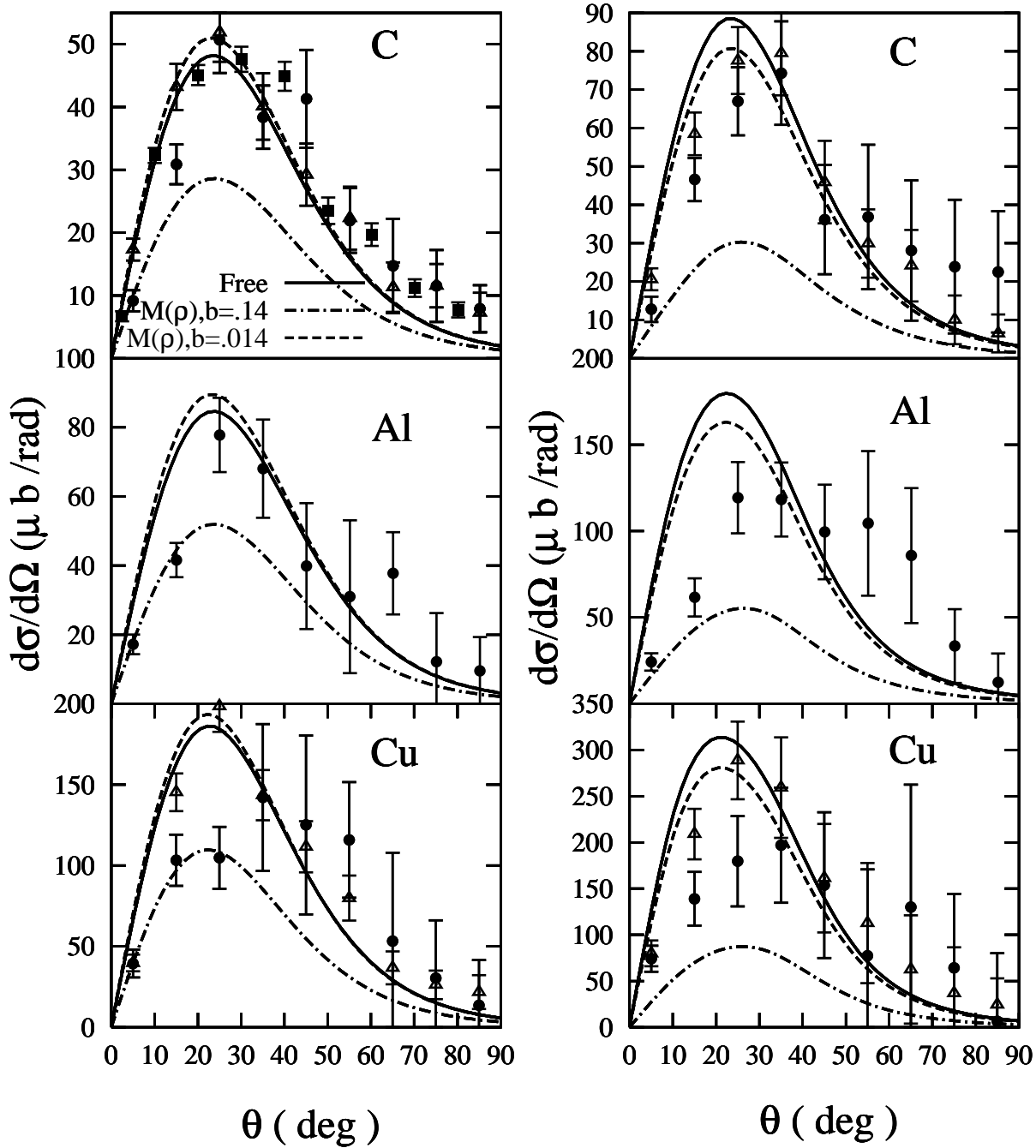


Fig.3

$$C(\gamma, \eta)$$

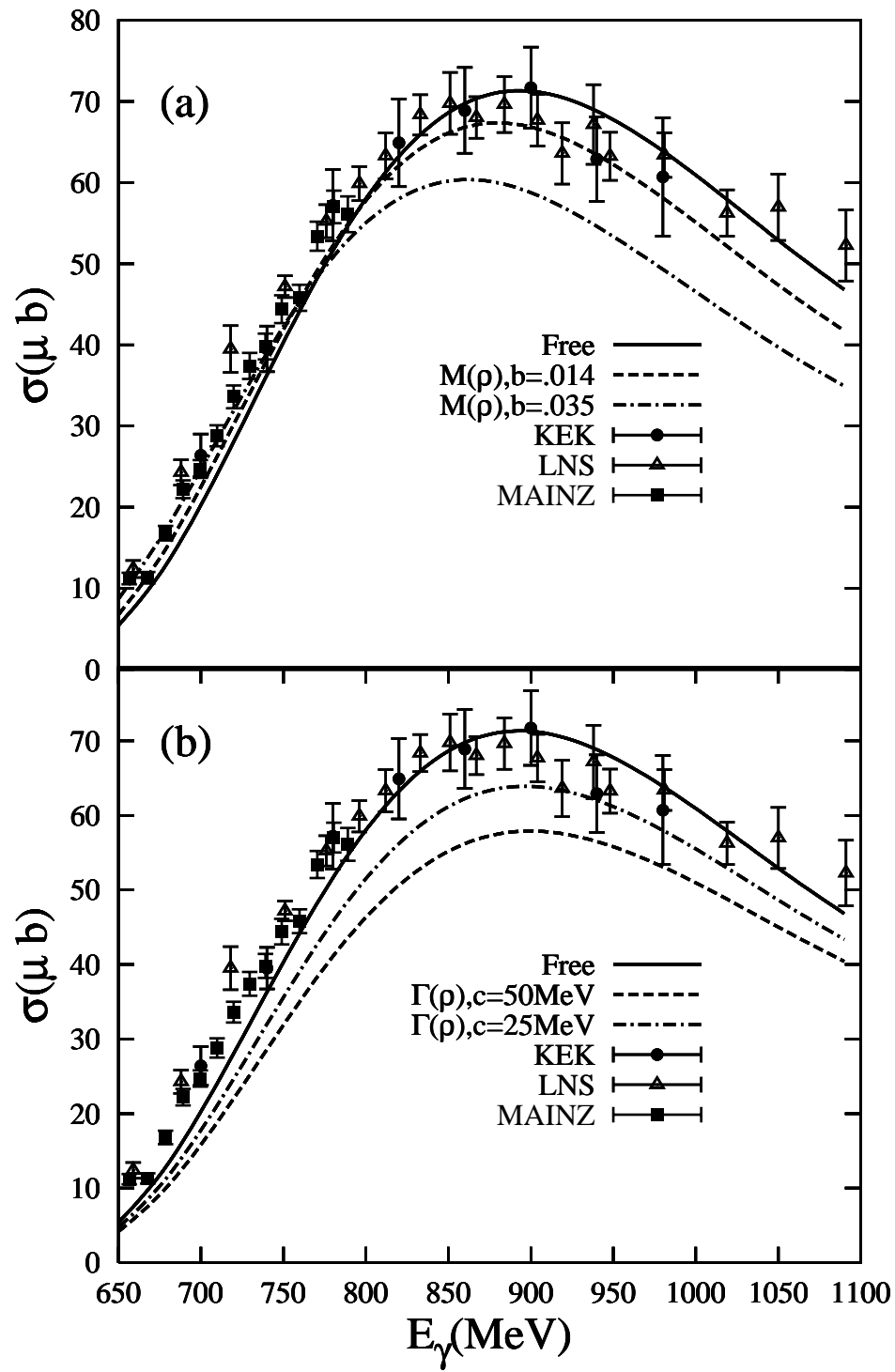


Fig.4

Al(γ, η)

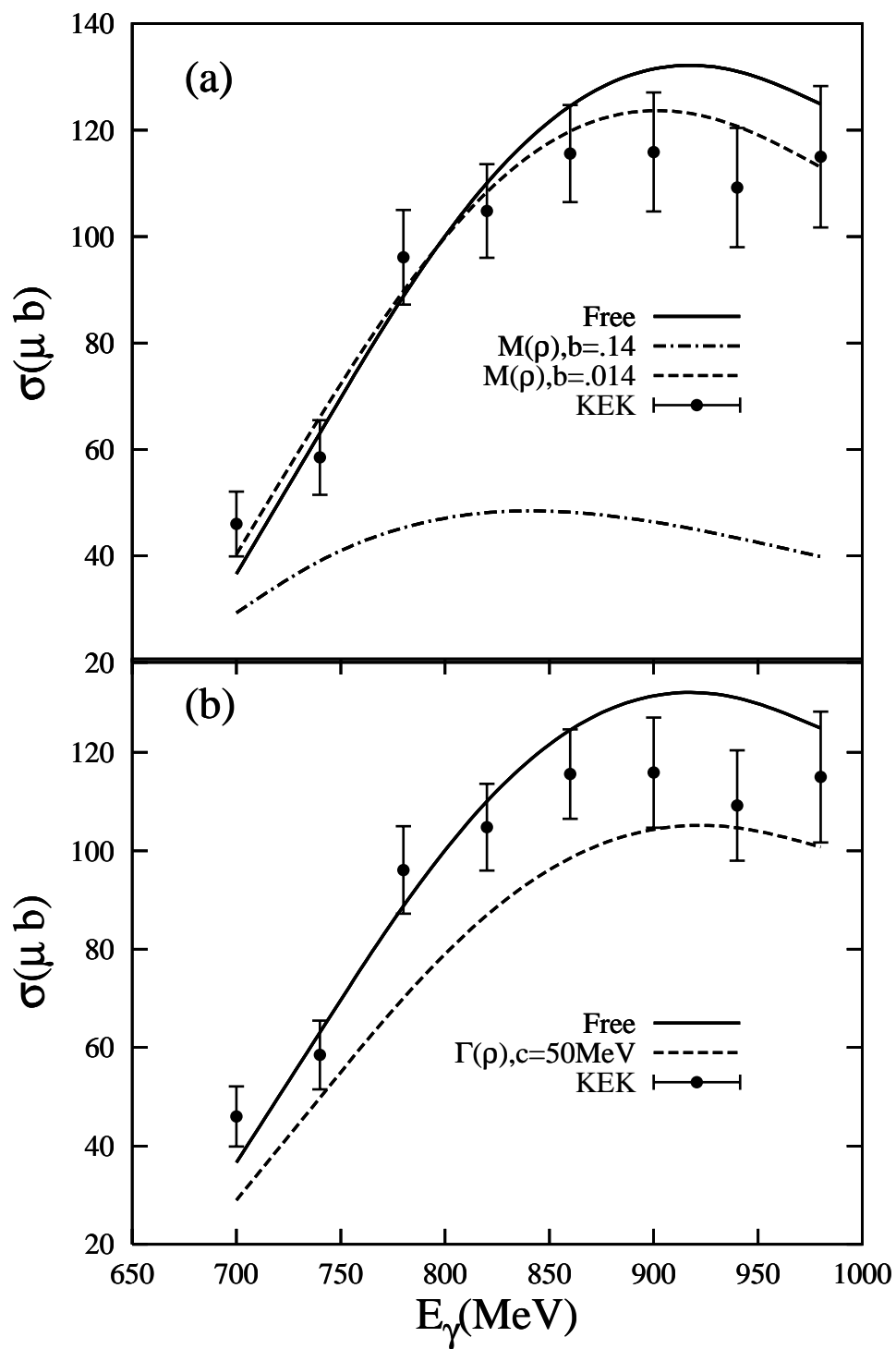


Fig.5

Cu(γ, η)

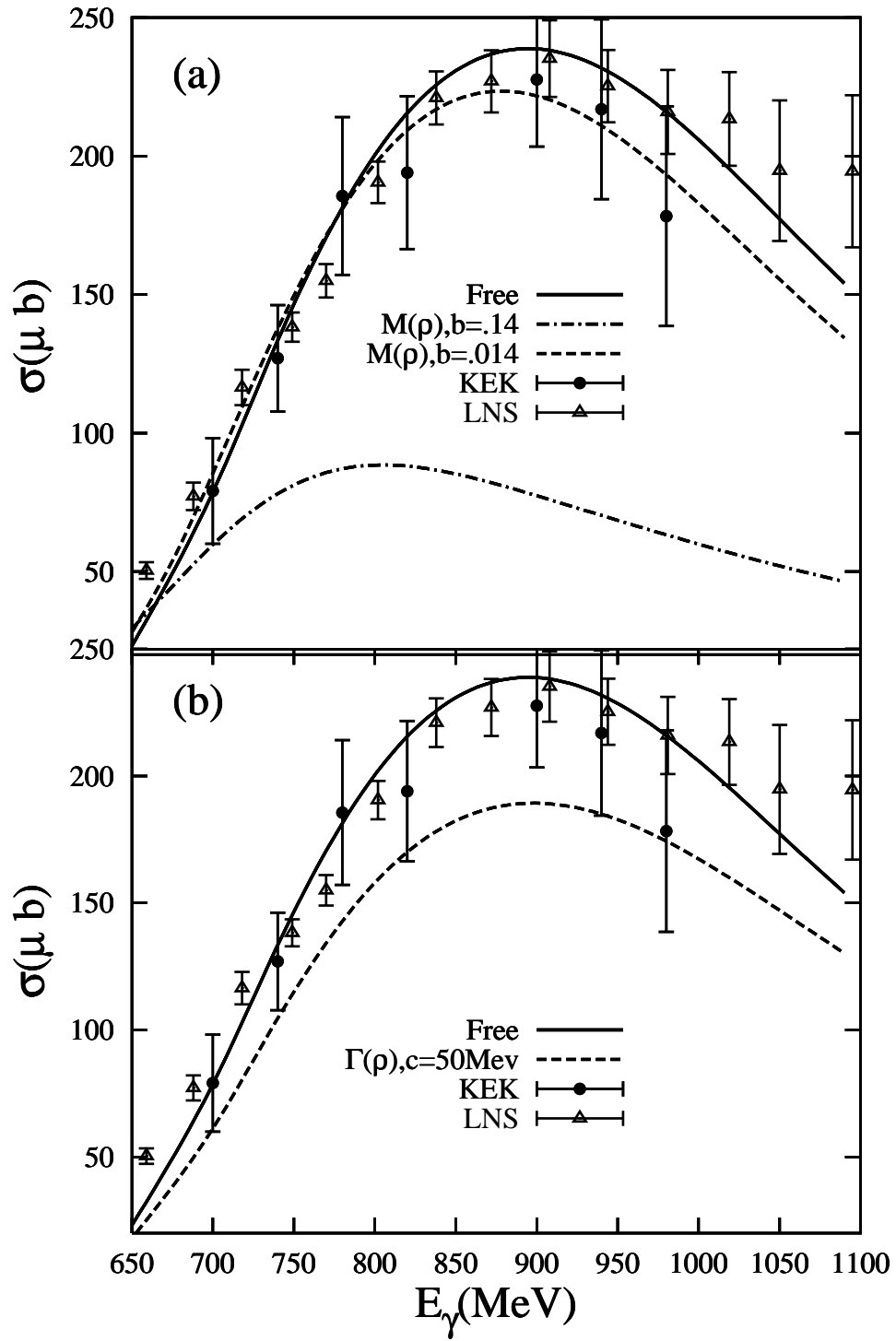


Fig.6

$C(\gamma, \eta)$

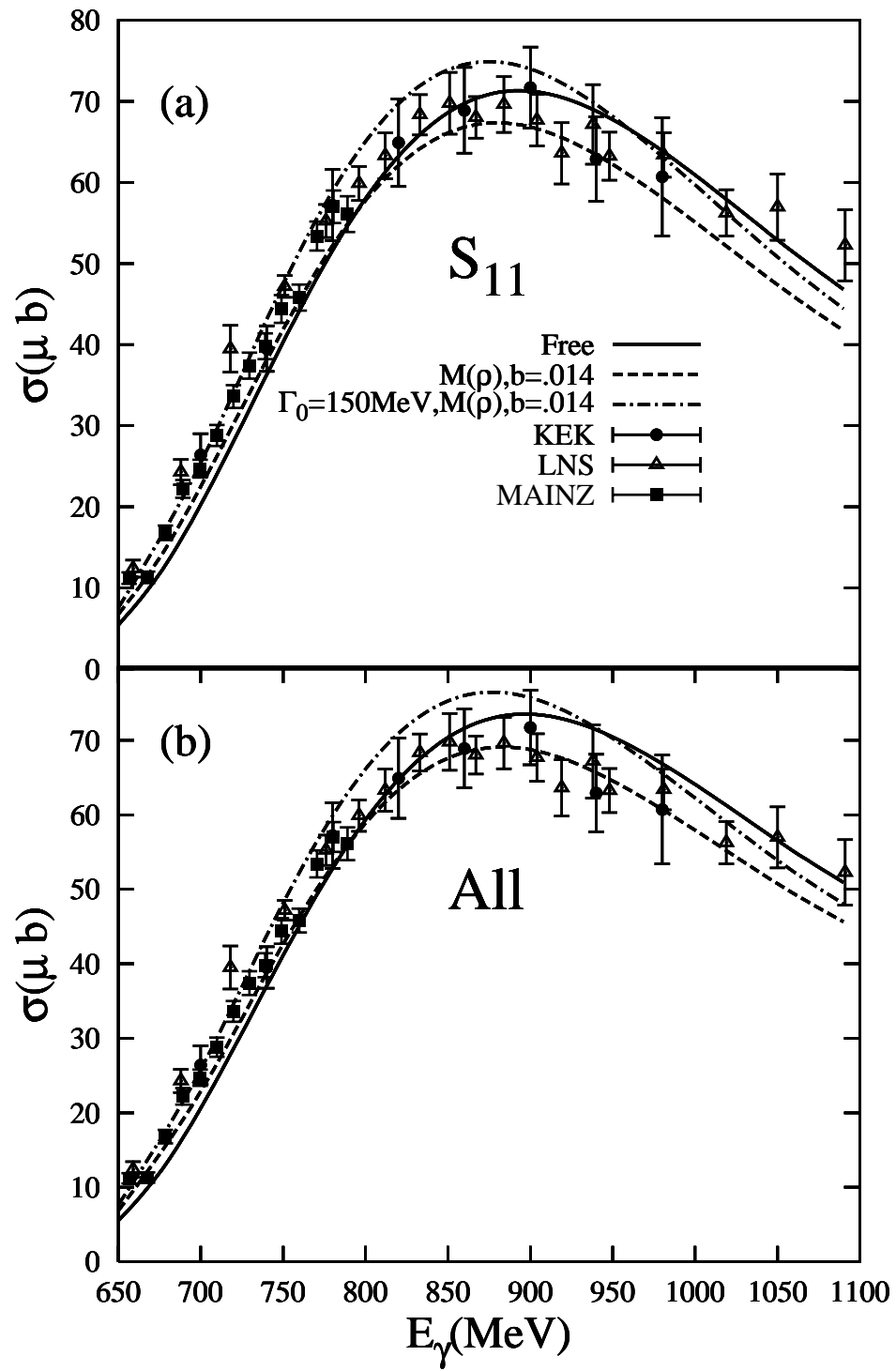


Fig.7

$C(\gamma, \eta)$

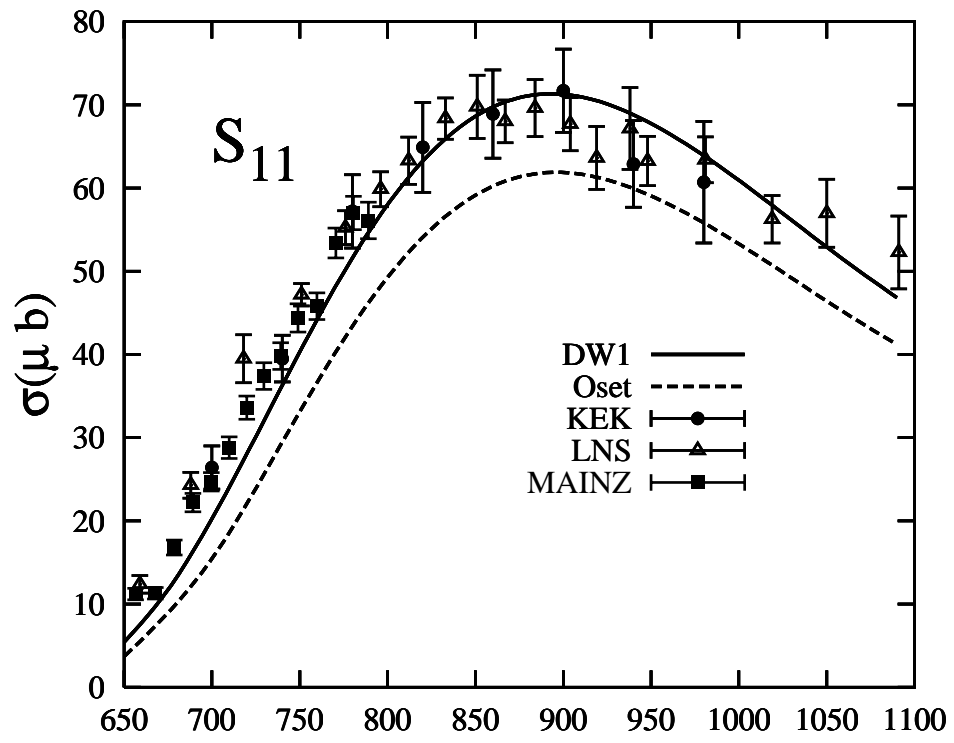


Fig.8